Fault-Related Thermal Springs: Water Origin and Hydrogeochemical Processes at Liquiñe Area (Southern Volcanic Zone, Chile)

Linda Daniele[1,2], Matías Taucare[1,2], Tomás Roquer[2,3], Benoît Viguier[1,2], Josefa Sepúlveda[2,3], Eduardo Molina[2,3], Gloria Arancibia[2,3], Diego Aravena[1,2], Mauricio Muñoz[1,2], Jorge Crempien[2,3], Antonio Delgado[4] and Diego Morata[1,2]

[1]Department of Geology, Facultad de Ciencias Físicas y Matemáticas, Universidad de Chile – 8370450 Santiago, Chile. [2]Andean Geothermal Center of Excellence (CEGA, Fondap-Conicyt 15090013) – 8370450 Santiago, Chile. [3]Structural Engineering and Geotechnical Department, Pontificia Universidad Católica de Chile – 7820436 Macul, Santiago, Chile. [4]Instituto Andaluz de Ciencias de la Tierra (CSIC-Universidad de Granada), 18100 Armilla (Granada), Spain.

Corresponding author: Matías Taucare (mtaucare@ing.uchile.cl)

Key Points:

- 15 thermal springs were surveyed along Liquiñe-Ofqui Fault System and Andean Transverse Faults in South Volcanic Zone (Chile).
- Thermal springs have a meteoric origin and its composition is driven by albite dissolution enhanced by deep volcanic gases (H_2S and CO_2).
- Regional (>50 km) and local (<50 km) assessment of fault control on water chemistry show differences with previous literature results.

Abstract

Geothermal activity in the Chilean Southern Volcanic Zone is strongly controlled by the regional Liquiñe-Ofqui Fault System (LOFS) and the Andean Transverse Faults (ATF). We analyzed fifteen thermal springs in the Liquiñe area to assess the origin and the main physicochemical processes related to the LOFS and ATF.

Major, minor and trace elements identify two defined clusters spatially related to the regional fault systems. In both clusters, ionic relationships suggest that the principal hydrogeochemical processes are mainly dominated by water-rock interactions. Factorial analysis provided two factors: i) F1 (65.1%), saturated by Cl^-, HCO_3^-, Na^+, SiO_2, Li, B and Cs, represents water-rock interaction processes driven by temperature in presence of CO_2; ii) F2 (28.5%) represented by SO_4^{-2} and Mo, represents a minor water-rock interaction enhanced by the presence of H_2S. Samples associated to the LOFS have high scores of both factors, while those from the ATF have only high factor 1 scores. Ionic ratios compared with literature data, clearly identify the samples spatially associated to the LOFS from the ones associated to the ATF with a fuzzy pattern.

Water stable isotopes values suggest a meteoric origin with small deviations from local meteoric isotopic line. CO_2 exchange with slightly high and low temperature water rocks interaction is present in most of the samples.

Our results indicate that groundwater circulation along faults is a complex process where different constraints influence the final hydeogeochemistry and reaction intensity. Finally, the established processes at Liquiñe area are not upscalable at the whole Southern Volcanic Zone.

Plain Language Summary

Geothermal springs are systems link the lithosphere, hydrogeological and atmospheric cycles. Generally, three key factors control the generation of thermal springs: heat sources, groundwater and reservoir lithology and structure. The geological setting of Chile suggests that it is very promising for geothermal development, indeed Chile, like others countries of Pacific Rim, presents several thermal manifestations mainly related to tectonic factors.

In the Chilean environments thermal waters, circulate and react throughout fractures networks. The geochemistry of thermal springs can allow to track the movement of these fluids in depth and can be used to inference the origin of spring waters, the relative water's ages and on the recharge and mixing processes. Further, it represents also a good way to better understand the functioning of the faults and its influence on geochemical organization of geothermal systems.

Our paper analyze fifteen thermal springs of the Liquiñe area (Southern Chile), to explore the influence of regional faults on the main physicochemical processes established for these samples. In addition, we compare our results with previous data and found that local scale processes associated to both fault system are not directly scalable to a more regional conclusion on LOFS and ATF thermal spring behavior.

1 Introduction

On the Earth's crust, fractures, including both joints and faults, are common features impacting a suite of geological processes serving both as barriers or high-permeability conduits for fluids, heat, and solute transport (Newell et al., 2008; Di Napoli et al., 2011; Bense et al., 2013; Townend et al., 2017; Patterson et al., 2018; Taillefer et al., 2018). Fractures can represent

an important control on fluids circulation and heat distribution, enhancing and focusing heat transfer and fluid flow (Townend et al., 2017; Patterson et al., 2018).

In the Andean Chilean Cordillera, the fluid circulation related to fractured rocks represents a potential for the exploration of groundwater and future exploitation of geothermal systems due to the specific geological and tectonic settings. In particular, within the Southern Volcanic Zone (SVZ, 33°-46ºS), the vast geological and tectonic features grants the possibility to analyze the interactions between faults and fluids circulation (Pérez-Flores et al., 2016). Different studies suggest that most of the several thermal springs in the SVZ are spatially related to the 1200 km long, NNE-striking Liquiñe-Ofqui Fault System (LOFS) and to the NW-striking Andean Transverse Faults (ATF) (Rosenau et al., 2006; Held et al., 2018; Pérez-Flores et al., 2016; Roquer et al., 2017; Tardani et al., 2016; Wrage et al., 2017). Held et al., (2018), Tardani et al., (2016) and Wrage et al., (2017) outline different isotopic signatures which reflect a strong component of meteoric water, with estimated reservoir temperature ranging between 80 to 150 ºC (Nitschke et al., 2018, Sánchez et al., 2013). Held et al., (2016, 2018) indicate residence times using CFC and Sr isotopic composition together with geophysical patterns (*i.e.* connection of the mid-crustal conductor to the ESE-WNW-striking fault zones), obtaining older ages up to 450-550 years. Sánchez et al., (2013) estimated reservoir maximum depth of ~2-3 km. Finally, Pérez-Flores et al., (2016) conclude that the LOFS would promote the constant circulation of hydrothermal fluids while the ATF would promote the storage of hydrothermal fluids.

Nevertheless, many mechanisms and processes could modify fluid composition even at local scale in such a complex hydrogeological context. All previous works, developed in the SVZ, analyze these thermal springs at the regional scale (>50 km). Although distinctive geochemical signatures between the thermal springs associated with the LOFS and the ATF have been found at the regional scale, the hypothesis that such distinctive chemical behavior may be also present at the local scale (<50 km) has still not been tested. Therefore, we propose the Liquiñe area (Fig. 1) as a case-study to downscale and analyze the hydrogeochemical processes, water origin and possible structural controls on thermal fluid geochemistry. At Liquiñe several small-spaced thermal springs outflow with different temperature (40-80ºC) and chemical composition. Moreover, in this zone both LOFS and ATF outcrops allow assessing how these fractures can influence the fluid circulation and the geochemical composition at local scale. During investigations carried out to evaluate the low enthalpy exploitation of the Liquiñe thermal springs, we perform a detailed hydrogeochemical and isotopic survey with the aim to assess the main physicochemical processes and role played by LOFS and ATF on groundwater circulation and thermal water geochemistry at the local scale. The general objective of this work is to analyze the scalability of the regional constraints on the geochemistry of thermal fluids to provide new understanding concerning the principal processes controlling flow circulation in the SVZ.

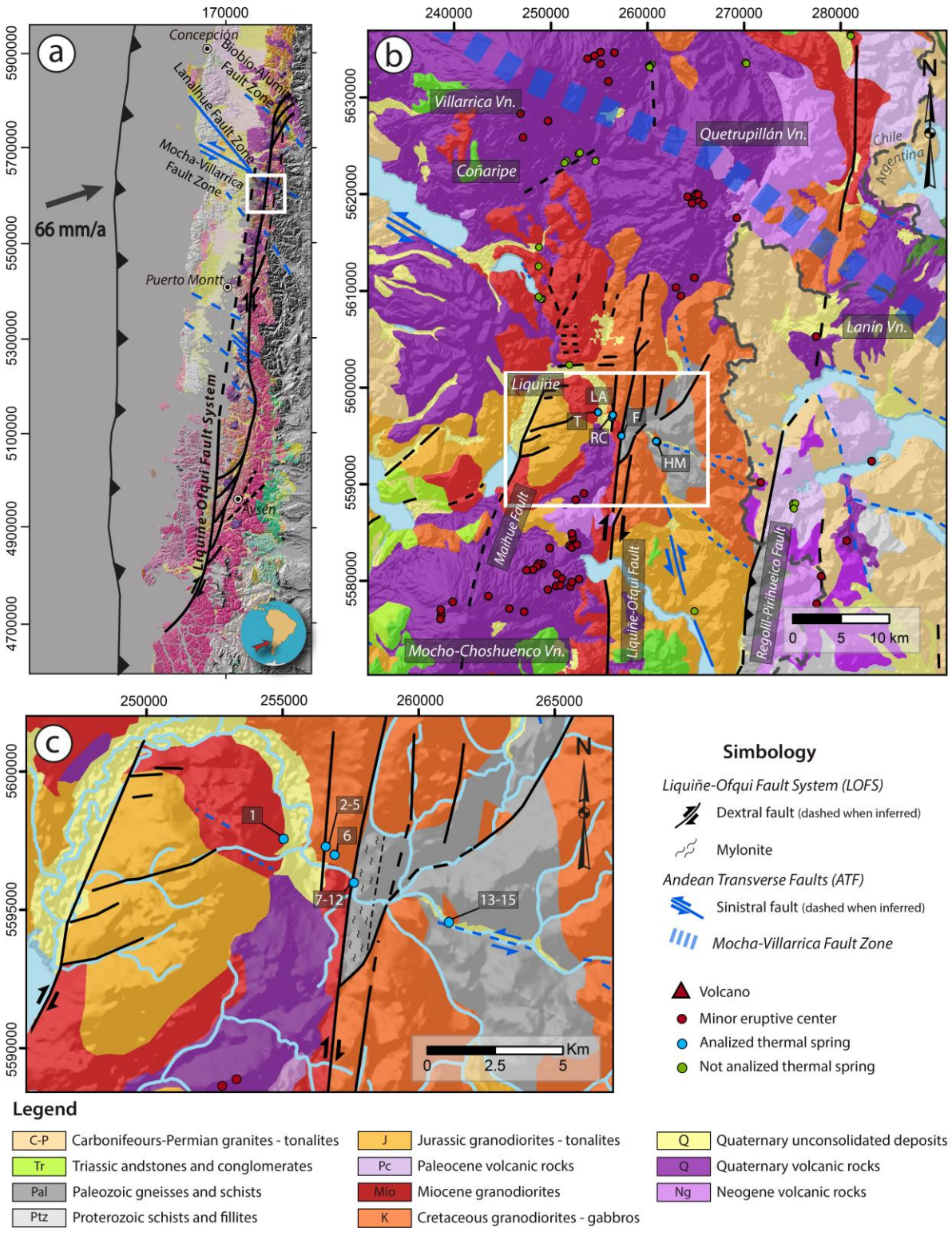

Figure 1. (a) Geological map of the Southern Andes Volcanic Zone (Modified from Pérez-Flores et al., 2016). Mainly structural features are shown: the Liquiñe-Ofqui Fault System and the Andean Transverse Faults. The arrow represents the convergence vector (66 mm/yr)

(Angermann et al., 1999). (b) Regional geological map showing the spatial relationships of the eruptive centers and thermal springs with respect major fault-systems. (c) Geological map of the study area (modified from Lara and Moreno, 2004). The location of sampled thermal springs are shown (LA = La Armada, T = Trafipan, RC = Rayen-Co, F = Fucha, HM = Hipolito Muñoz).

2 Geological and Tectonic Setting

The SVZ corresponds to the central segment of the Andean volcanic arc in Chile (Fig. 1a). The tectonic setting of the SVZ is driven mainly by oblique subduction between the Nazca and South American plates (*e.g.* Cembrano and Lara, 2009). Deformation is partitioned into margin-parallel and margin-orthogonal components, accommodated within the fore and back-arc regions and the arc region respectively (Cembrano et al. 1996; Pérez-Flores et al. 2016; Rosenau et al. 2006). Within the volcanic arc in the SVZ, crustal deformation is controlled by the Liquiñe-Ofqui Fault System (LOFS) and the Andean Transverse Faults (ATF). The LOFS is a regional-scale active fault system with a trace length of 1200 km. It has main alignments NS to NNE-striking dextral and dextral-reverse faults parallel to the arc, and subsidiary NE to ENE-striking dextral and dextral-normal duplexes with brittle movement mainly developed in the last 6 Ma (Fig. 1b) (Arancibia et al., 1999; Rosenau et al., 2006; Cembrano and Lara, 2009). The ATF include a group of NW to WNW-striking sinistral and sinistral-reverse faults (Fig. 1b) (Melnick et al., 2006; Rosenau et al., 2006). Both groups of faults and fractures have strongly deformed the rocks of the North Patagonian Batholith (NPB) outcropping in the studied area (*e.g.* Cembrano and Lara, 2009), around the Liquiñe village. Quaternary volcanic rocks from SVZ are mainly emplaced over Jurassic to Miocene tonalitic to granodioritic-tonalitic intrusive bodies from the NPB (*e.g.* Munizaga et al., 1988), which intrude Paleozoic intrusive and metamorphic rocks (Lara and Moreno, 2004).

In the study zone, at least fifteen thermal springs (Fig. 1c) outflow mainly related to: (1) fractures affecting granodiorites rocks along the damage zone of the LOFS (Trafipan (nº1), La Armada (nº2-5), Rayen-Co (nº6)); (2) fractures associated to mylonitic bands in the core of LOFS (Fucha (nº7-12)) and (3) semi-consolidated fluvial sediments overlying Cretaceous granodiorites, which occur in a N70W-trending valley (Hipolito Muñoz (nº13-15)), presumably associated with the ATF. From a hydrogeological point of view, the main circulation occurs within fractured and faulted lithologies as well as within sediments along rivers. Due to the thickness of these sediments, potential aquifers should be scarce.

3 Sampling and Methods

During September 2018, we sampled a set of 15 thermal springs, 2 surficial and 1 meteoric water samples. Electrical conductivity (EC), temperature and pH were measured in situ. Water samples were filtered using 0.45 µm Millipore filters, unacidified samples were collected for anion analysis, and acidified samples (with Suprapur® Nitric acid) for cations and trace elements analysis. Additionally, unfiltered samples were collected for isotopic analysis. All samples were stored in pre-cleaned polyethylene bottles at 4 °C.

Major, minor and trace elements were analysed in the laboratories of the Andean Geothermal Centre of Excellence (CEGA, Chile). Cl^-, SO_4^{-2} and F^- contents were determined by Ion Chromatography (IC, 861 Compact IC Metrohm) with a detection limit of 0.01, 0.025 and 0.002 ppm, respectively. SiO_2, Na^+, K^+, Ca^{2+}, and Mg^{2+} were measured by Atomic Absorption Spectrophotometry (F-AAS, Perkin-Elmer PinAAcle 900F), with detection limits of 0.8, 0.03,

0.12, 0.02 and 0.004 ppm, respectively. Li, B, As, Rb, Mo and Cs contents were determined by Inductively Coupled Plasma Mass Spectrometry (ICP-MS, Thermo iCAP Q) with detection limits of 0.02, 0.07, 0.02, 0.001, 0.002 and 0.0003 ppb, respectively. The HCO_3^- concentration (ppm) were determined by Volumetric Titration using the method proposed by Giggenbach and Goguel (1989). Isotopes analysis was carried out at the *Estación Experimental de Zaidín* (CSIC, Spain). The $\delta^{18}O$ and $\delta^{2}H$ were analysed by Finnigan Delta Plus XL mass spectrometer. The experimental error was ±0.1% and ±1.1% for $\delta^{18}O$ and $\delta^{2}H$ values, respectively.

In order to assess the hydrogeochemical processes controlling thermal water composition and its relationship to the fault setting, we used major, minor and trace elements plots, ionic ratios and ionic relationships. Surficial and rain water samples are plotted as a reference. To evaluate water sampled origin and processes, a reliable local meteoric water line based on available dataset close to Liquiñe zone has been used (IAEA/WMO, 2019) to calculate the annual weight means of $\delta^{18}O$ and $\delta^{2}H$ and define the local meteoric water line, hereafter "regional meteoric water line".

Multivariate statistical analyses within the hydrogeochemical data were used to identify spatial patterns among the water samples and the parameters controlling their composition (*e.g.* Moya et al., 2015; Negri et al., 2018). The methods used in this study are Hierarchical Cluster Analysis (HCA) and Factorial Analysis (FA). HCA was performed to estimate groups of samples with similarities using a linkage rule. To obtain distance measures with linkage rules we employed the Euclidian distance combined with Ward's method (*e.g.* Moeck et al., 2016). The implementation of these linkage rules yields the most distinctive geochemical clusters (Güler et al., 2002). Graphically, the results have been depicted as a dendrogram, where the similarity between clusters is expressed by the link distance at which the branches are connected. FA generated a small number of uncorrelated factors that help identify the relationships between the geochemical variables. This statistical method explains most of the variance without a substantial loss of information (Daniele et al., 2008; Negri et al., 2018). Kaiser's criterion was used to determine the factors using eigenvalues higher than 1. Bartlett and KMO tests were calculated to quantify the significance of FA. The components were rotated using the varimax method, to maximize the variance of the squared loading for each factor. Finally, the weight of the variables of each factor is called "loading", and each factor is associated with at least one variable. Loading values >0.5 define the representative variables for the factors. All statistical analyses were performed using Cl^-, SO_4^{-2}, HCO_3^-, Na^+, SiO_2, Li, B, Mo and Cs data using the IBM SPSS Statistics Software V22.0. To minimize or eliminate the presence of outliers and the high biased typical for compositional data (*e.g.* Filzmoser et al., 2009), log-transformation was applied on raw data prior to multivariate analysis.

Sample Id	Location Name	Fault Domain	T°C	pH	EC (µS/cm)	Eh (mv)	Major Elements (ppm)									Trace Elements (ppb)					
							SiO_2	Cl^-	SO_4^{-2}	HCO_3^-	F^-	Na^+	K^+	Ca^{+2}	Mg^{+2}	Li	B	As	Rb	Mo	Cs
1	T	LOFS	36.9	8.7	349	151.0	46.1	20.78	58.04	54.9	0.69	51.66	1.58	8.90	0.723	19.68	271.51	34.53	7.27	8.84	4.98
2	LA	LOFS	68.3	9.1	417	-409.5	96.3	17.74	66.86	91.5	1.19	68.50	2.34	3.81	*bdl*	55.58	128.72	9.91	21.63	10.22	18.95
3	LA	LOFS	60.0	9.2	376	-329.2	87.0	16.07	60.22	85.4	1.04	61.11	2.12	4.59	*bdl*	52.01	119.08	10.20	19.25	11.37	16.61
4	LA	LOFS	32.3	7.9	116	-118.8	33.4	4.27	17.11	48.8	0.27	14.10	0.81	6.22	0.892	11.99	32.55	2.46	4.39	2.75	3.24
5	LA	LOFS	52.9	8.9	345	-63.4	80.0	14.44	58.76	61.0	0.96	54.18	2.02	4.55	0.118	46.76	110.07	9.54	17.90	10.71	15.23
6	RC	LOFS	61.7	9.2	420	-438	95.9	16.29	68.96	73.2	1.20	69.75	2.82	3.40	*bdl*	59.87	134.71	10.68	21.26	11.75	20.04
7	F	LOFS	19.1	7.3	114	30.5	25.0	4.61	16.59	54.9	0.23	12.95	2.46	9.91	0.989	4.38	29.76	1.81	2.09	3.37	0.69
8	F	LOFS	43.5	9.7	364	-365.2	58.2	19.39	68.35	79.3	1.07	63.25	2.48	4.69	*bdl*	20.37	138.05	10.09	6.79	13.82	2.98
9	F	LOFS	24.9	9.5	268	191.3	44.4	15.16	47.19	67.1	0.76	43.68	2.33	7.10	0.330	15.50	98.10	6.93	5.15	10.98	2.25
10	F	LOFS	38.9	9.7	354	-350.8	57.7	19.45	68.32	79.3	1.11	63.25	0.53	4.30	*bdl*	20.39	139.55	10.23	6.76	13.90	2.96
11	F	LOFS	31.8	9.1	240	-265.0	44.3	14.64	47.06	54.9	0.75	42.00	1.06	6.89	0.448	14.61	96.74	6.90	4.85	10.06	2.10
12	F	LOFS	24.1	9.8	317	-304.1	53.8	17.51	62.55	54.9	0.98	55.23	1.18	5.65	0.119	18.05	124.40	9.02	5.73	12.65	2.36
13	HM	ATF	60.8	8.9	486	-417.5	90.4	32.71	57.93	128.1	2.63	92.50	1.04	2.39	*bdl*	119.05	311.62	1.25	24.80	3.13	35.47
14	HM	ATF	79.4	8.9	452	-457.5	86.3	29.74	50.48	128.1	2.39	100.00	0.82	2.37	*bdl*	111.82	284.82	1.40	21.08	5.10	27.73
15	HM	ATF	75.1	8.8	480	-414.1	83.9	30.18	48.64	128.1	2.45	82.00	0.92	2.77	0.100	119.09	308.17	1.69	21.86	3.42	29.00
16	Surficial	-	9.3	7.6	39	360.1	14.0	1.04	0.98	30.5	0.05	2.05	0.60	5.30	0.673	1.01	*bdl*	0.13	1.14	0.73	0.15
17	Surficial	-	12.3	7.1	23	-	10.0	1.01	0.66	17.7	*bdl*	1.53	0.67	2.53	0.460	0.06	2.37	0.09	1.15	0.24	0.08
18	Meteoric	-	12.5	6.5	14	-	*bdl*	1.35	0.88	17.7	*bdl*	0.82	2.69	0.37	0.001	0.06	2.52	0.10	2.44	1.42	0.08
*bdl: Below detection limit			Detection limits (ppm):				0.8	0.01	0.025	0.1	0.002	0.03	0.12	0.02	0.004	0.02	0.07	0.02	0.001	0.002	0.0004

Table 1. Chemical analysis of thermal, surficial and meteoric water samples. (T: Trafipan, LA: La Armada, RC: Rayen-Co, F: Fucha, HM: Hipolito Muñoz, LOFS: Liquiñe-Ofqui Fault System, ATF: Andean Transverse Faults).

4 Results

4.1 Major elements

The analytical results obtained are summarized in Table 1. Electrical Conductivity (EC) of thermal waters range between 114 µS/cm to 486 µS/cm. Measured temperatures lie between 19.1°C (nº7) and 79.4°C (nº14) and pH varies between 7.3 (nº7) and 9.8 (nº12). Surficial water (22.7-39.3 µS/cm) and rain water (13.7 µS/cm) are less mineralized with pH values of 7.1-7.6 (nº16-17) and 6.4 (nº18). Measured Eh values in thermal water are mostly negative, except for Trafipan (151 mV), and two Fucha samples (30.3 mV and 191.3 mV). These results suggest that in general, there is an anoxic groundwater flow, which circulates back to the thermal springs.

Thermal waters are mostly HCO_3^--Na^+ and SO_4^{-2}-Na^+ water types. Surficial waters are HCO_3^--Ca^{+2} and rain water fall in HCO_3^--Na^+ area. Major ions have concentrations up to 150 ppm (HCO_3^-) and samples nº13-14 and 15 (Hipolito Muñoz thermal springs) are those with the highest ionic content.

To show the presence of different trends in the concentrations of measured elements, major elements and F^- were plotted versus temperature data (Fig. 2). The positive correlation of most of the analyzed ions indicates that salinity is temperature related. Nevertheless, sulphate does not show a clear positive correlation with temperature, indeed samples nº2, 6, 8 and 10 with very different temperatures, has similar SO_4^{-2} content (>66 ppm).

Chloride ion allows to identify different clusters in the sampled thermal waters. As showed in figure 3 most of major ions samples have a strong positive correlation with Cl^- content. Most of the samples (nº1-6 and nº8-12) with 10-20 ppm of Cl^- are grouped in the central part of the plots. Low temperature thermal waters (nº4 and nº7) seem more geochemically related

to surficial/meteoric waters as shown in the SiO_2 concentration plot. Samples from Hipolito Muñoz (nº 13-15) thermal springs have the highest Cl^- contents, with a maximum of 32.71 ppm (nº13). Comparing all plots in figure 3, Hipolito Muñoz samples show maximum concentration of all plotted ions except for SO_4^{-2} and Ca^{+2} contents. Indeed, $SO4^{-2}$ does not show a clear correlation, while Ca^{+2} shows negative correlation related to Cl^-.

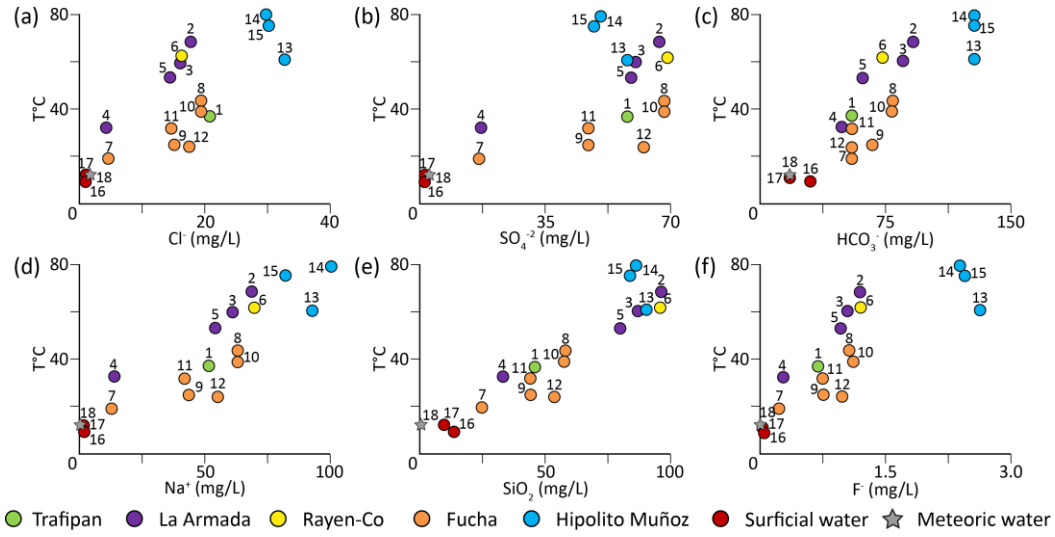

Figure 2. Major ions concentrations [mg/l] vs. surface temperatures [°C] of water samples.

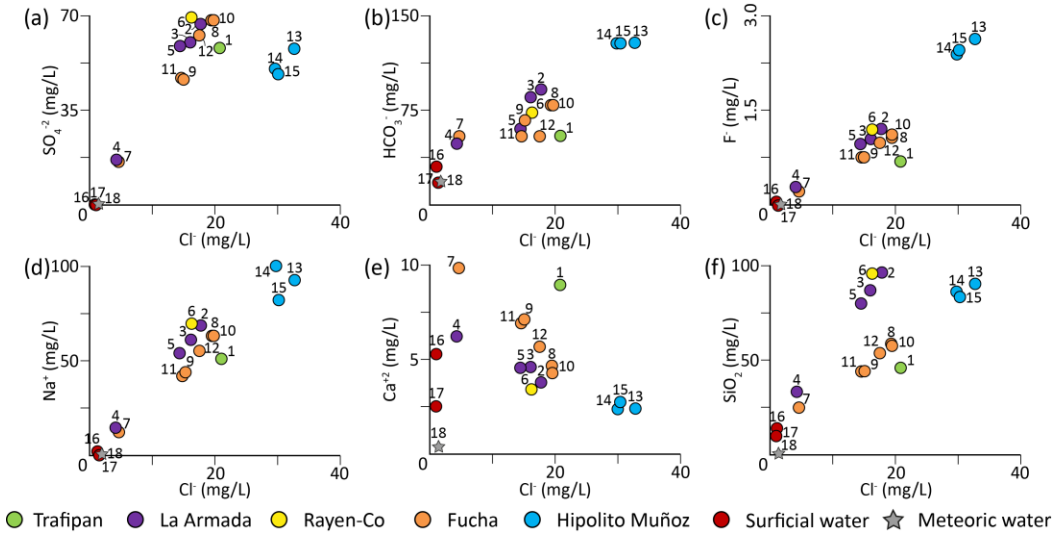

Figure 3. Major ions [mg/l] vs. Cl^- [mg/l] concentrations of water samples.

4.2 Trace elements

Trace elements analysed for this study include Li (4.38-119.09 ppb), B (29.76-311.62 ppb), As (1.25-34.53 ppb), Rb (2.01-24.70 ppb), Cs (0.69-35.47 ppb) and Mo (2.75-13.90 ppb) as shown in Table 1. Most of the trace elements show a positive correlation with Cl^-, with the exception of As and Mo (Fig. 4). Li, Rb, and Cs display a clear positive correlation that indicates

two different trends. Cold samples from Fucha (nº7) and La Armada (nº4) are very close to surficial and meteoric samples. Trafipan (nº1) and hot Fucha samples (nº7-12) define a trend where the trace elements increase is less dependent to salinity. On the other hand, La Armada (nº2,3,5) and Rayen-Co (nº6) samples point to a clear Li, Rb and Cs increase up to the Hipolito Muñoz samples, which have the highest concentrations. As, B and Mo show one general trend with Cl-, where it is not possible to separate the Fucha and La Armada samples. Most of the samples have a clear increase of As, B and Mo contents with Cl^-, but Hipolito Muñoz samples, with the highest Li, B, Rb and Cs concentrations have, lower As and Mo contents. Trace elements plotted in figure 4 corroborate the clusters identified with major ions.

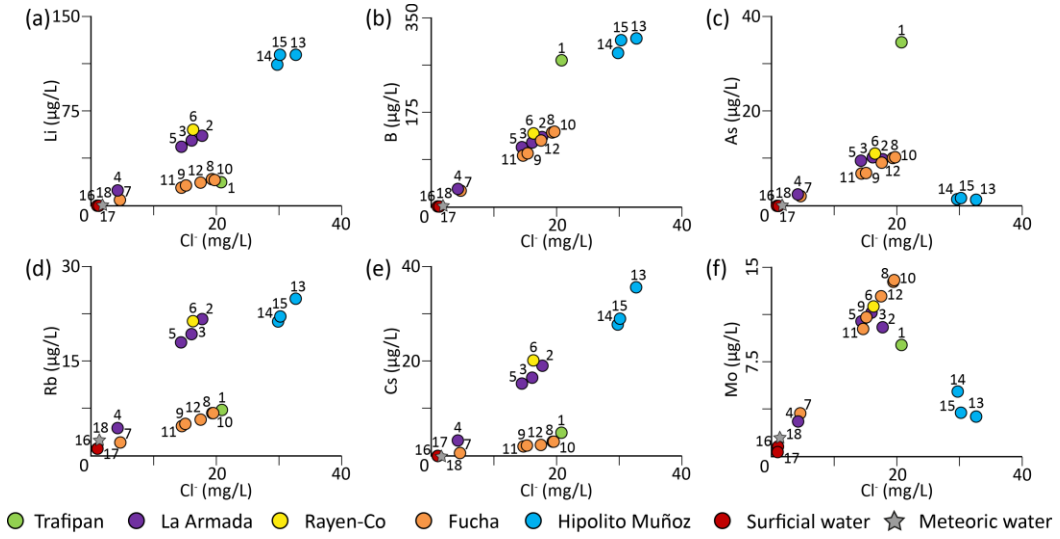

Figure 4. Trace elements vs. surface temperatures and Cl^- [mg/l] concentrations of water samples.

4.3 Multivariate statistical analysis

The results of the HCA are displayed as a dendogram with phenon line defined at a linkage distance of 7.5. HCA group the samples in three principal clusters (Fig. 5) strengthen the binary plot results. Thermal waters are mainly grouped in the first cluster that consists of $SO4^{-2}$-Na^+ thermal waters with up to 20.78 ppm of Cl^-, less of 91.5 ppm of HCO_3^- and the highest Mo and As contents. The second cluster includes Hipolito Muñoz samples, which are HCO_3^--Na^+ thermal waters with highest EC and temperature values. The third cluster group the coldest thermal samples (nº4 and nº7) with surficial and meteoric water that show the lowest EC and temperature values. The high linkage distance between proposed clusters indicates a statistically significant difference, which suggests physicochemical processes of different nature and/or intensity.

The FA results performed using significant chemical elements. Bartlett (0.0) and KMO (0.77) values ensure the significance of FA. Two factors with eigenvalues above one explain 93.6% of the total variance. Factor 1 (65.1%) represents the strong association between Cl^-, HCO_3^-, Na^+, SiO_2, Li, B and Cs. Factor 2 (28.5%) is saturated with a positive correlation between SO_4^{-2} and Mo. The two factors suggest a different source for the variables of each factor. The factor scores for each sample are shown in Table 2.

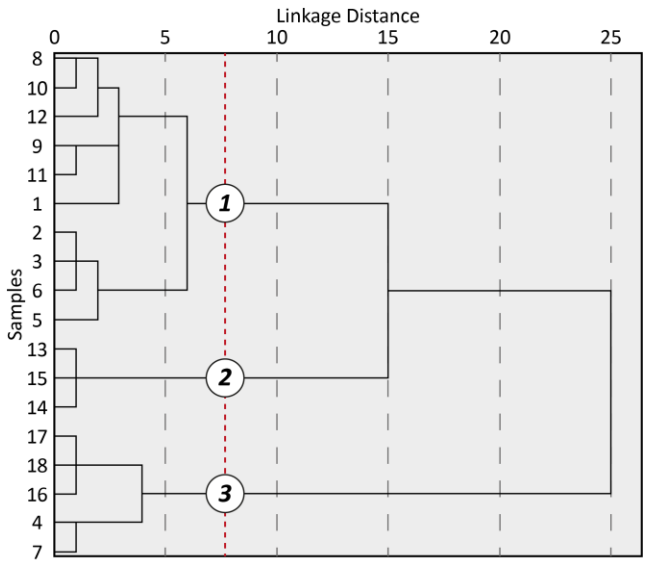

Figure 5. HCA dendogram for the 18 samples. Segmented line defines phenon line at a linkage distance of 7.5.

Parameters	Components	
	Factor 1	Factor 2
Cl^-	**0.90**	0.33
SO_4^{2-}	0.52	**0.85**
HCO_3^-	**0.95**	0.19
Na^+	**0.88**	0.46
SiO_2	**0.79**	0.51
Li	**0.98**	-0.04
B	**0.91**	0.17
Mo	0.01	**0.99**
Cs	**0.83**	0.46
Variance (%)	65.10	28.51
Cumulative variance (%)	65.10	93.61

Table 2. Factorial analysis with Varimax rotation. These two factors describe 92.6% of the data set variance. Loading values >0.5 are marked in bold.

4.4 Isotope composition

Results of $\delta^{18}O$ and $\delta^{2}H$ of thermal waters range from -10.43‰ to -2.34‰ and from -64.86‰ to -45.35‰ respectively (Table 3). Values of $\delta^{18}O$ and $\delta^{2}H$ for surficial water range between -6.58‰ and -46.26‰, and for rainwater, the contents lie within -1.10‰ and -15.41‰. The relationship between $\delta^{2}H$ and $\delta^{18}O$ of collected samples is shown in figure 6 where data were plotted with Regional Meteoric Water Line (RMWL) drawn using regional data (IAEA, 2015), and with Global Meteoric Water Line (GMWL) (Craig, 1961). Samples fall on both side of the LMWL and GMWL, indicating depletion and enrichment relative to those lines. Only the samples from Fucha springs, associated to LOFS, are sideways on the CO_2 exchange trend line. Hipolito Muñoz samples (nº13-15) deviate towards degassing and mineral exchange line, with more variable $\delta^{18}O$ values, ranging between -8.60 and -2.34 and $\delta^{2}H$ values are within -64.2 and

-45.35. The rest of the samples are slightly to the right of the LMWL and GMWL. Surficial and meteoric water ($\delta^{18}O$ = -6.58 and -1.17; $\delta^{2}H$ = -46.26 and -15.41) lie close to the LMWL.

Sample Id	Location Name	Fault Domain	Ionic Ratios (meq/L)						Stable Isotopes	
			rSO_4/rCl	$rHCO_3/rCl$	rNa/rSO_4	$rNa/rHCO_3$	rLi/rCl	rB/rCl	δD (VSMOW)	$\delta^{18}O$ (VSMOW)
1	T	LOFS	2.06	1.54	1.86	2.50	0.0048	0.129	-60.09	-8.42
2	LA	LOFS	2.78	3.00	2.14	1.99	0.0160	0.071	-63.48	-8.23
3	LA	LOFS	2.76	3.09	2.12	1.90	0.0165	0.073	-60.38	-7.34
4	LA	LOFS	2.95	6.63	1.72	0.77	0.0143	0.075	-55.98	-7.49
5	LA	LOFS	3.00	2.46	1.93	2.36	0.0165	0.075	-61.57	-9.17
6	RC	LOFS	3.12	2.61	2.11	2.53	0.0188	0.081	-64.81	-9.83
7	F	LOFS	2.65	6.91	1.63	0.63	0.0048	0.063	-59.20	-8.73
8	F	LOFS	2.60	2.38	1.93	2.12	0.0054	0.070	-64.22	-10.28
9	F	LOFS	2.30	2.57	1.93	1.73	0.0052	0.064	-63.15	-9.57
10	F	LOFS	2.59	2.37	1.94	2.12	0.0054	0.071	-64.86	-10.43
11	F	LOFS	2.37	2.18	1.87	2.03	0.0051	0.065	-63.87	-9.95
12	F	LOFS	2.64	1.82	1.85	2.67	0.0053	0.070	-64.60	-9.92
13	HM	ATF	1.31	2.28	3.34	1.92	0.0186	0.094	-45.35	-2.34
14	HM	ATF	1.25	2.50	4.14	2.07	0.0192	0.094	-56.72	-7.43
15	HM	ATF	1.19	2.47	3.52	1.70	0.0202	0.101	-64.20	-8.60
16	Surficial	-	0.69	17.03	4.38	0.18	0.0050	0.001	-	-
17	Surficial	-	0.48	10.18	4.85	0.23	0.0003	0.023	-	-
18	Meteoric	-	0.48	7.62	1.95	0.12	0.0002	0.018	-	-

Table 3. Ionic ratios and isotopic analysis of thermal, surficial and meteoric water samples. (T: Trafipan, LA: La Armada, RC: Rayen-Co, F: Fucha, HM: Hipolito Muñoz, LOFS: Liquiñe-Ofqui Fault System, ATF: Andean Transverse Faults).

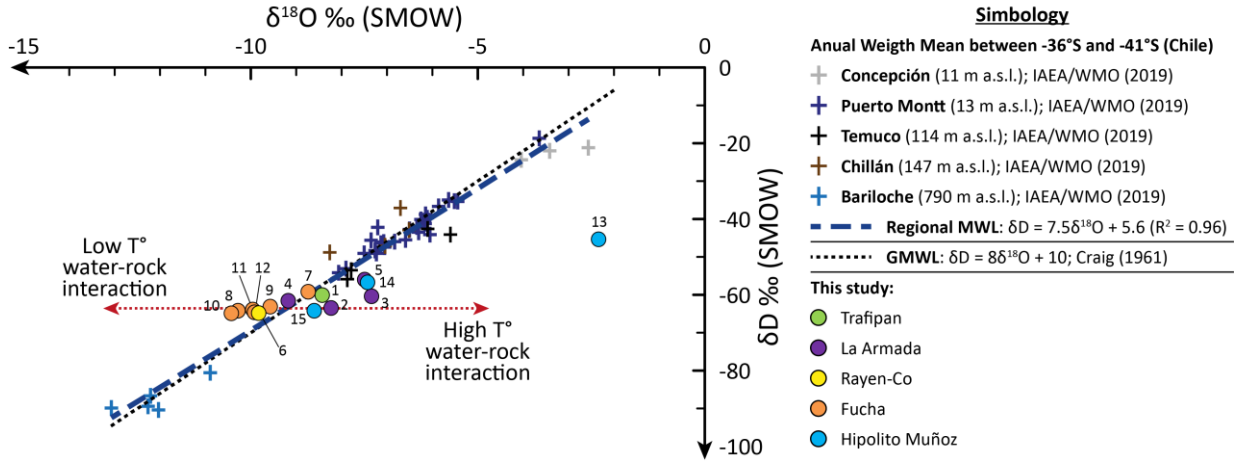

Figure 6. Relationship between $\delta^{2}H$ vs. $\delta^{18}O$ for water samples.

5 Discussion

Faults may play an important control in water upflow/outflow (*e.g.* Townend et al., 2017) as proved by the emergence of hot springs along LOFS and ATF traces. However, the nature and intensity of hydrogeochemical processes resulting from hydrogeological LOFS and ATF control at local scale are still unclear. At such local scale, a well-developed fault-fracture network

favours the development of hydrothermal cells, and promotes the advection of fluids and heat (Roulleau et al. 2018). In addition, the study of hot fluid flow through fault zones can provide strong constraints on geothermal exploration (*e.g.* Taillefer et al., 2017, 2018). In the next subsections, the nature and intensity of hydrogeochemical processes and their relationship with LOFS and ATF are discussed.

5.1 Hydrogeochemical processes and thermal water origin

Several chemical reactions may influence water hydrogeochemistry and major ions can help to trace water-rock interaction processes (*e.g.* Daniele et al., 2013; Vallejos et al., 2015; Negri et al., 2018) and/or the presence of dissolved gases (Reyes et al. 2010).

According to the geochemical composition, chloride and other analysed ions allow us to separate the samples into different clusters. Two samples, nº4 and nº7 have a close hydrogeochemical association with meteoric and surficial water samples indicating that significant mixing with meteoric and shallow water takes place. Salinity of samples (*i.e.* Cl^-) is strongly related to temperature as indicated in figure 3. The positive correlations between the different ions, temperature and salinity suggest that the chemical composition of thermal waters is mainly controlled by water-rock interactions, enhanced by temperature. The identified water types HCO_3^--Na^+ and SO_4^{-2}-Na^+ evidences the primary role of those ions and consequently will be used to identify the water-rock interaction processes. All samples have an excess of Na^+ when compared to the Cl^- concentration (Fig. 7a) indicating that different hydrogeochemical processes release Na^+ in the sampled waters.

The albite (Na-plagioclase) weathering may be at the origin of the Na^+ found in the waters, enhanced by temperature and the presence of H_2S and CO_2 geothermal gases (Arnórsson, 1986). Thus, albite weathering under these conditions (equation 1 and 2) releases an as 2:1 and 1:1 proportion amount of Na^+ with respect to SO_4^{-2} and HCO_3^- (Fig. 7b), respectively.

$$2NaAlSi_3O_8 + H_2S + 2O_2 \leftrightarrow 2Na^+ + 6SiO_2 + 2AlO(OH) + SO_4{}^{-2} \quad (1)$$

$$NaAlSi_3O_8 + CO_2 + 2H_2O \leftrightarrow Na^+ + 3SiO_2 + Al(OH)_3 + HCO_3{}^- \quad (2)$$

All thermal water, with the exception samples nº4 and nº7, fall between the 1:1 and 1:2 molar lines (Fig. 7b), indicating that albite dissolution from the considered reactions is the source of these ions. As both reactions release Na^+, the contribution of each one is assessed by subtracting the corresponding anion to the total Na^+ content (Fig. 7c and 7d). In the [Na^+-HCO_3^-] versus [SO_4^{-2}] diagram (Figure 7c) most of thermal waters plot along and close to the 2:1 stoichiometry line, suggesting the presence of H_2S. In opposition, the meteoric and surface samples, with the coldest thermal water sampled at Fucha (nº7) and La Armada (nº4), show negative values which confirm the meteoric and surface influence in those samples. The Hipolito Muñoz thermal waters also show in this plot a Na^+ excess. In turn, the [Na^+-$2SO_4^{-2}$] versus [HCO_3^-] diagram (Fig. 8d) depict a 1:1 trend of most of the thermal water, which suggests that the albite dissolution in presence of CO_2 is taking place within the fracture networks. The amounts of [Na^+-HCO_3^-] in water explained by albite weathering and enhanced by H_2S (Fig. 7c) seem to be subordinate to the weathering in presence of CO_2 (Fig. 7d). In fact, most of the

samples fit better the 1:1 line in figure 7c, where the Hipolito Muñoz samples show a larger excess in sample nº15, which has the highest temperature.

Thus, albite weathering in presence of H_2S and CO_2 explains the principal concentration of the samples. The systematic position of meteoric, surficial and cold thermal springs (nº4 and nº7) in all diagrams point to the strong temperature control on the intensity of water-rock interaction and helps to assess the possible origin of these cold thermal springs. The fact that cold thermal springs are spatially located very close to the hot ones evidences the complex groundwater circulation along faults and fracture networks, which attests the first order control of structures on groundwater processes, as the percolation and mixing with surficial waters.

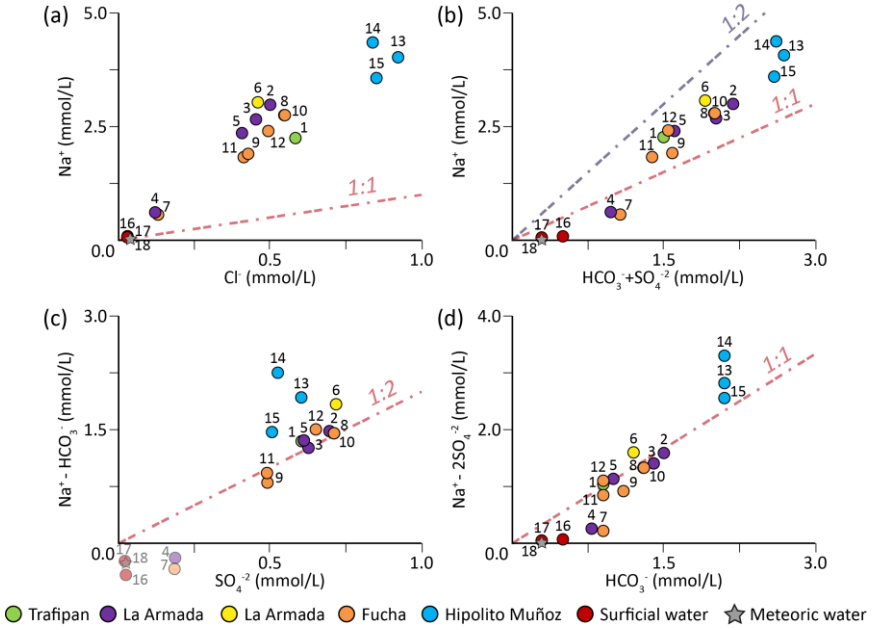

Figure 7. Molar relationships between Na^+ [mmol/l] vs. major anions [mmol/l]. Dashed lines show the stoichiometry ratios.

Major ions do not display significant differences between Fucha and La Armada samples, which systematically plot close in the diagrams shown in figures 2 and 3. Nevertheless, trace elements such as Li, Rb and Cs separate visibly the samples of both springs (Fig. 4a, d and e). The relative position of Fucha, Trafipan and La Armada in the plots of figures 2 (d, f) and 3 (a, d, e) suggests that water-rock processes may act with different intensity, probably due to different temperature range between thermal springs. In fact, Fucha temperature samples range between 19.1-43.5ºC, while La Armada is between 32.3-68.3ºC and Rayen-Co is 61.7ºC. The observed differences may be due to the fault zone springs outflow as the La Armada and Rayen-Co samples (n°2-6) outflow along the damage zone, while Fucha samples (n°7-12) outflow along the LOFS fault core. As pointed out by different authors (*e.g.* Caine et al., 1996; Faulkner et al., 2010; Gudmundsson et al., 2010; Choi et al., 2016), rocks are more permeable in the damage zone than in the fault core, suggesting that groundwater and heat circulation is more favourable in damage zones. However, the temperature range and chemical composition of the samples indicates a complex set of paths along faults and fractures networks.

The multivariate statistical approach confirms the same differences obtained from binary plot evaluation. The dendrogram groups the samples separating three distinct clusters. Fucha and Trafipan thermal waters form a cluster that is related to La Armada and Rayen Co (nº8-12 and nº1) samples. The Hipolito Muñoz thermal springs are related to these with a larger linkage distance, which implies a significant difference in the physicochemical processes that occur in both thermal waters. Cold thermal springs from Fucha and La Armada (nº4 and nº7) are linked to meteoric and surficial water, confirming the more surficial origin of those waters.

The FA identified two factors interpreted as the process of albite dissolution in presence of CO_2 and H_2S. In detail, the factor 1, with high values for most of the analysed variables, is associated with dissolution in presence of CO_2 and factor 2 is associated with H_2S albite dissolution. SiO2 and Na have similar values in both factors because they are product of both dissolution processes (equations 1 and 2). The highest variance of F1 (65.1%) compared with F2 (28.5%) suggests that albite dissolution in presence of CO_2 is the main process. In figure 8, the factor scores calculated for each sample are shown. The scores allow to differentiate the samples and the processes that characterize each one. Thus, the meteoric and surficial water plus the cold samples from Fucha and La Armada have negative scores for both factors. That means that the albite dissolution is not the principal process in those samples, given the surficial origin of samples nº4 and nº7. The composition of Hipolito Muñoz samples according to our interpretation is driven by albite dissolution in presence of CO_2 (positive F1) with no H_2S involvement (negative F2). On the other hand, Fucha and one sample collected at La Armada (nº5) seem to be related to an albite dissolution with H_2S as indicated by the positive scores of F2, as well as the absence of CO2 presence (negatives F1 scores). Trafipan, Rayen-Co and La Armada (nº2 and n°3) have a composition related to both albite dissolution processes. Still, the F2 positive values, higher than F1 ones, suggest that albite dissolution in presence of H_2S is the principal water-rock interaction process. Based on fundamental natural processes controlling kinetic and equilibrium of water stable isotopes (*e.g.* Karolytė et al., 2017), our data slightly deviated both sides of GMWL and LMWL lines. It indicates that a CO_2 exchange, mineral reaction at high and low temperature and degassing occur in the analysed water.

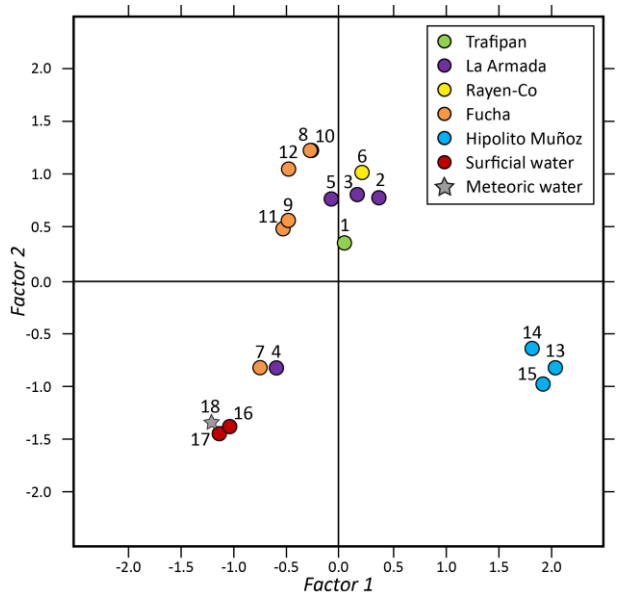

Figure 8. Plot of factorial scores on each sample.

5.2 Regional hydrogeochemical assessment

Along and across the SVZ, crustal fluid flow and reservoir presence are mainly controlled by structurally-driven permeability, as already indicated by different authors (Lara et al., 2008; Sánchez et al., 2013; Pérez-Flores et al., 2016; Wrage et al., 2017; Held et al., 2018). At 38ºS, the basement changes from volcano sedimentary rocks to crystalline plutonic rocks of the Patagonian batholith. Patagonian batholith have been related to a more vertical fluid circulation (Sánchez et al., 2013) due to the formation of fault-fracture networks under strike-slip deformation (Held et al., 2016). Different authors use physicochemical composition, ionic relationships and ratios, to discriminate the thermal waters controlled by LOFS and ATF faults (Sánchez et al., 2013; Wrage et al., 2017). Sánchez et al. (2013) indicate that pH and B/Cl ratio help to separate ATF (pH<8; high B/Cl) from LOFS (pH>8; low B/Cl) thermal waters. Wrage et al. (2017) discriminate the LOFS and ATF thermal waters using Cl/B ratio concluding that ATF (low Cl/B) and LOFS (high Cl/B) exert a significant influence on the Cl and B concentration in thermal water.

The results of this local scale thermal water survey, discussed considering the LOFS and ATF systems, point out to some differences with published literature using the pH and B/Cl ratios. Most of thermal waters analyzed in this manuscript have pH values above 8.0 with a slight difference in pH values of LOFS samples (pH=8.64-9.79) and those related to samples collected at ATF (pH=8.80-8.93) sites. Samples nº4 and nº7 (pH=7.29-7.90) are an exception, because their origin is linked to surficial water.

Ionic ratios versus Cl^- are plotted in figure 9, along with available published data from different authors (Sánchez et al. 2013; Wrage et al. 2017; Held et al. 2018). The B/Cl diagram (Fig. 9f) does not separate clearly our samples. In fact, the B/Cl values for LOFS and ATF samples do not exceed 0.129. So, unlike Sánchez et al. (2013) and Wrage et al. (2017), results suggest that B/Cl ratio is not a useful hydrogeochemical signature to differentiate the structural control at the local scale. The SO_4/Cl (Fig. 9a), Na/SO_4 (Fig. 9c) and Li/Cl (Fig. 9e) ratios are especially interesting, since they clearly separate the ATF (nº 13-15) from LOFS samples. Namely, the ATF samples have SO_4/Cl, Na/SO_4 and Li/Cl maximum values of 1.5, 4.14 and 0.02 respectively. These samples appear separated systematically from LOFS samples in all graphs displayed in figure 9. Considering also literature data, the ATF samples exhibit a fuzzier pattern with respect to the LOFS samples. Moreover, few samples associated to the ATF by other authors show similar ionic ratios with those related to the LOFS shown in this study (Fig. 9). The Li content seem to be the key element to separate samples even along LOFS, in fact Trafipan and Fucha have a lower Li/Cl ratio. The observed difference seem to be related to samples temperature variation. Hence, the ionic ratios helped to identify the clusters defined in this study by means of major, minor and trace elements, as well as the use of multivariate statistical analysis techniques.

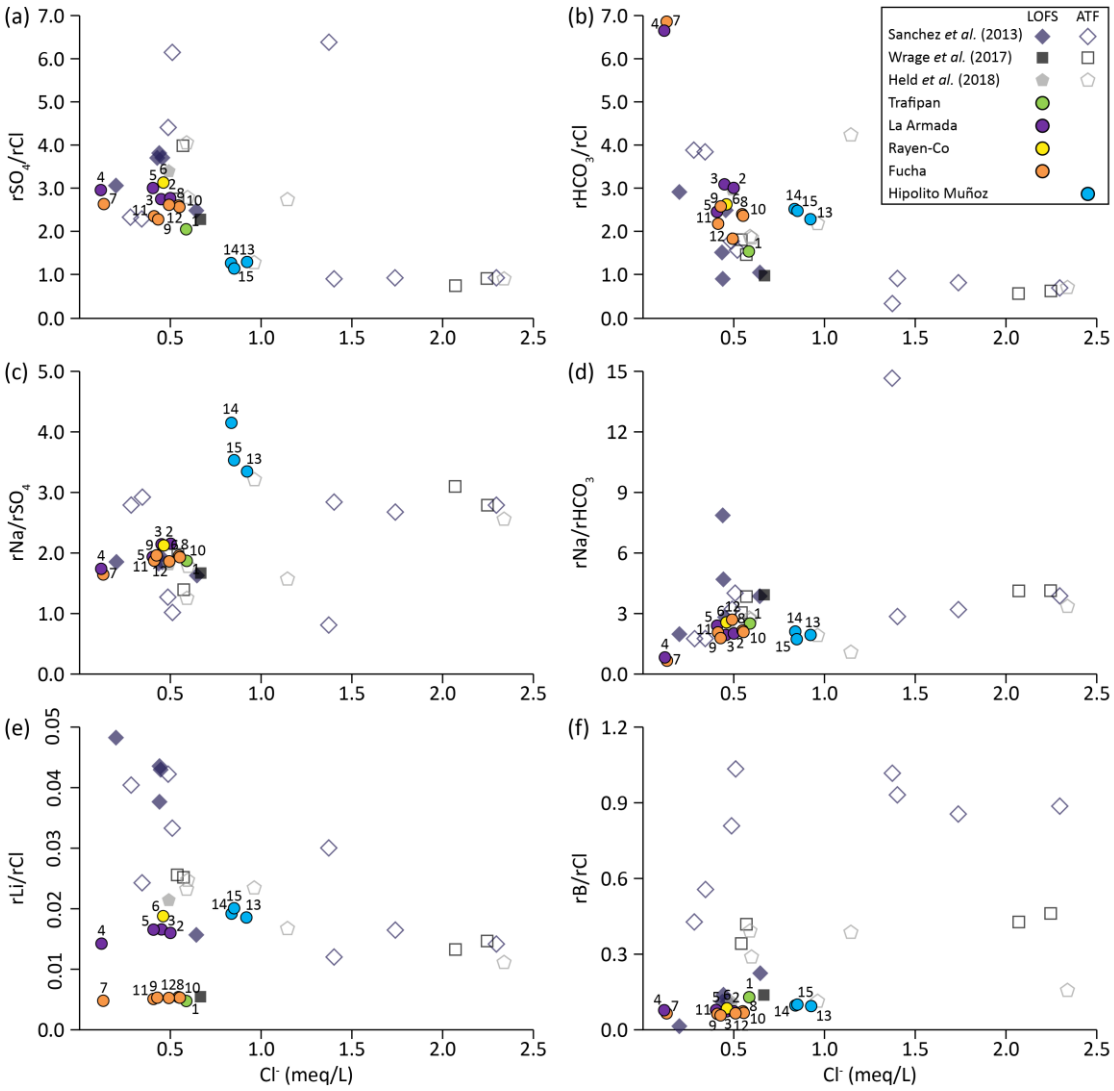

Figure 9. rSO4/rCl, rHCO3/rCl, rNa/rSO4, rNa/rHCO3, rLi/rCl and rB/rCl ratios vs. Cl- [meq/l] in thermal, surficial and meteoric water samples (r means that concentrations are in meq/l).

Finally, a schematic conceptual model of the processes detected in the study area was constructed using the geochemical data, hydrogeological and structural setting (Fig. 10). The analyzed samples are meteoric water flowing through fractures and sediments. Water–rock interaction takes place in both fault settings in presence of deep hydrothermal gases that are responsible also for heat contribution. Processes intensity and heat contribution appear related to fault zone architecture as shown by samples outflowing along core and damaged zone of LOFS. In fact, samples along LOFS damage zone (La Armada and Rayen-Co) have the highest temperatures and SiO_2, Li, Rb and Cs concentrations compared with samples from mylonitic bands in the core of LOFS (Fucha). The Hipolito Muñoz samples, associated to ATF, have the maximum temperatures measured in this study as well as the highest major and trace elements concentrations, except for SO_4, As and Mo contents, probably due major CO2 gas contribution. Therefore, it is suggested that a hydraulic connection between the surface and deep flow occurs in this area. Moreover, the average residence times of 450-550 years (Held et al., 2018) may facilitate the identified hydrogeochemical processes.

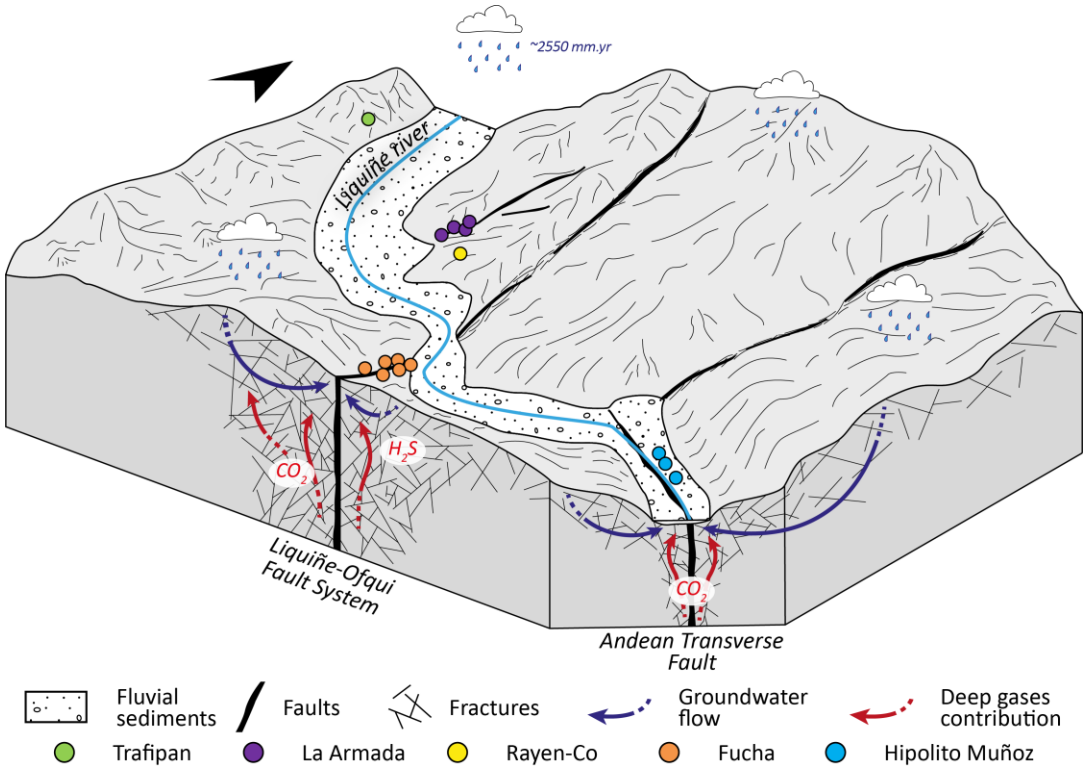

Figure 10. Simplified conceptual model illustrating the processes occurring in the sampled thermal water of Liquiñe area. Arrows represent groundwater flow directions.

6 Conclusions

The thermal water composition sampled in the Liquiñe area indicates that the origin of the dissolved solutes is produced by water-rock interaction, in the presence of geothermal gases such as H_2S and CO_2. The principal hydrogeochemical process identified is the albite dissolution, a widely common mineral in granitic rocks, which are present in the study area. The salinity of the samples divides the samples in two clusters, which are spatially associated with the two main groups of faults. The stable isotopic composition respect to LMWL and GMWL suggest that thermal waters have a meteoric origin, while the slight isotopic shift suggests that changes are related to gases and mineral exchanges.

At the local scale, faults have a key role in the processes identified, as well as the intensity with which they occur in the analyzed samples. Along the LOFS, the water-rock interaction is enhanced by H_2S and CO_2, while along the ATF the same process is boosted by CO_2. Comparing the local scale results (<10 km) with literature data at regional scale (>50 km), we found that the thermal waters related to ATF exhibit a fuzzier pattern with respect to the LOFS samples. In contrast, the samples related to LOFS in this study show similarity with complied ATF data.

In the Liquiñe zone, it has been possible to identify in detail the processes and a compositional variation within a small domain of outflowing thermal springs along the two fault systems. The results indicate the complexity of groundwater circulation along fault zones, even at a local scale. Thus, processes at the local scale are not necessarily replicable at the regional

scale. Finally, the study area is promising for geothermal energy direct use projects. The authors are actively engaged to develop local enterprises that will contribute to the socioeconomic development of the region.

Acknowledgments

The authors acknowledge the support of CONICYT FONDAP nº 15090013 (Andean Geothermal Center of Excellence, CEGA), FONDEQUIP EQM120098, FONDECYT nº 1170569 and nº 1180167, for funding this research. The PhD studies of Taucare and Roquer are funded by CONICYT – Beca Doctorado Nacional n° 21160325 and 21171178, respectively. We are grateful to Verónica Rodriguez, who performs the water chemical analysis at CEGA labs.

All the data used in this paper are listed in Tables 1-3 and may be download from the OpenEI Datasets (link in Supporting Information).

Supporting Information

https://openei.org/datasets/dataset/52e8e03f-bd4c-446f-b4b0-5d3fcd7555a5/resource/abf0e891-30ea-467a-8bf6-75de3a138e64/download/tables.xlsx

References

Angermann, D., Klotz, J., Reigber, C., 1999. Space-geodetic estimation of the nazca-south america euler vector. Earth and Planetary Science Letters 171, 329–334. https://doi.org/10.1016/S0012-821X(99)00173-9

Arancibia, G., Cembrano, J., Lavenu, A., 1999. Transpresión dextral y partición de la deformación en la Zona de Falla Liquiñe-Ofqui, Aisén, Chile (44-45°S). Andean Geology 26, 3–21. https://doi.org/10.5027/andgeov26n1-a01

Arnórsson, S., 1986. Chemistry of gases associated with geothermal activity and volcanism in Iceland: A review. Journal of Geophysical Research: Solid Earth 91, 12261–12268. https://doi.org/10.1029/JB091iB12p12261

Bense, V.F., Gleeson, T., Loveless, S.E., Bour, O., Scibek, J., 2013. Fault zone hydrogeology. Earth-Science Reviews 127, 171–192. https://doi.org/10.1016/j.earscirev.2013.09.008

Caine, J., Evans, J., Forster, C., 1996. Fault zone architecture and permeability structure. Geology 24, 1025–1028. https://doi.org/10.1130/0091-7613(1996)024<1025:FZAAPS>2.3.CO;2

Cembrano, J., Hervé, F., Lavenu, A., 1996. The Liquiñe Ofqui fault zone: a long-lived intra-arc fault system in southern Chile. Tectonophysics 259, 55–66. https://doi.org/10.1016/0040-1951(95)00066-6

Cembrano, J., Lara, L., 2009. The link between volcanism and tectonics in the southern volcanic zone of the Chilean Andes: A review. Tectonophysics 471, 96–113. https://doi.org/10.1016/J.TECTO.2009.02.038

Choi, J.H., Edwards, P., Ko, K., Kim, Y.S., 2016. Definition and classification of fault damage zones: A review and a new methodological approach. Earth-Science Reviews 152, 70–87. https://doi.org/10.1016/j.earscirev.2015.11.006

Craig, H., 1961. Isotopic Variations in Meteoric Waters. Science (New York, N.Y.) 133, 1702–3. https://doi.org/10.1126/science.133.3465.1702

Daniele, L., Bosch, A.P., Vallejos, A., Molina, L., 2008. Geostatistical Analysis to Identify Hydrogeochemical Processes in Complex Aquifers: A Case Study (Aguadulce Unit, Almeria, SE Spain). AMBIO A Journal of the Human Environment 37, 249–254. https://doi.org/10.1579/0044-7447(2008)37[249:GATIHP]2.0.CO;2

Daniele, L., Vallejos, Á., Corbella, M., Molina, L., Pulido-Bosch, A., 2013. Hydrogeochemistry and geochemical simulations to assess water-rock interactions in complex carbonate aquifers: The case of Aguadulce (SE Spain). Applied Geochemistry 29, 43–54. https://doi.org/10.1016/j.apgeochem.2012.11.011

Di Napoli, R., Martorana, R., Orsi, G., Aiuppa, A., Camarda, M., De Gregorio, S., Gagliano Candela, E., Luzio, D., Messina, N., Pecoraino, G., Bitetto, M., De Vita, S., Valenza, M., 2011. The structure of a hydrothermal system from an integrated geochemical, geophysical, and geological approach: The Ischia Island case study. Geochemistry, Geophysics, Geosystems 12. https://doi.org/10.1029/2010GC003476

Faulkner, D.R., Jackson, C.A.L., Lunn, R.J., Schlische, R.W., Shipton, Z.K., Wibberley, C.A.J., Withjack, M.O., 2010. A review of recent developments concerning the structure, mechanics and fluid flow properties of fault zones. Journal of Structural Geology 32, 1557–1575. https://doi.org/10.1016/j.jsg.2010.06.009

Filzmoser, P., Hron, K., Reimann, C., 2009. Univariate statistical analysis of environmental (compositional) data: Problems and possibilities. Science of The Total Environment 407, 6100–6108. https://doi.org/10.1016/J.SCITOTENV.2009.08.008

Giggenbach, W.F., Goguel, R.L., 1989. Collection and analysis of geothermal and volcanic water and gas discharge. Department of Scientefic and Industrial Research, Chemistry Division, 1989.

Gudmundsson, A., Simmenes, T.H., Larsen, B., Philipp, S.L., 2010. Effects of internal structure and local stresses on fracture propagation, deflection, and arrest in fault zones. Journal of Structural Geology 32, 1643–1655. https://doi.org/10.1016/j.jsg.2009.08.013

Güler, C., Thyne, G.D., McCray, J.E., Turner, A.K., 2002. Evaluation of graphical and multivariate statistical methods for classification of water chemistry data. Hydrogeology Journal 10, 455–474. https://doi.org/10.1007/s10040-002-0196-6

Held, S., Schill, E., Pavez, M., Díaz, D., Muñoz, G., Morata, D., Kohl, T., 2016. Resistivity distribution from mid-crustal conductor to near-surface across the 1200 km long Liquiñe-Ofqui Fault System, southern Chile. Geophysical Journal International 207, 1387–1400. https://doi.org/10.1093/gji/ggw338

Held, S., Schill, E., Schneider, J., Nitschke, F., Morata, D., Neumann, T., Kohl, T., 2018. Geochemical characterization of the geothermal system at Villarrica volcano, Southern Chile; Part 1: Impacts of lithology on the geothermal reservoir. Geothermics 74, 226–239. https://doi.org/10.1016/J.GEOTHERMICS.2018.03.004

IAEA/WMO, 2019. Global Network of Isotopes in Precipitation. The GNIP Database [WWW Document]. URL http://www.iaea.org/water

Karolytė, R., Serno, S., Johnson, G., Gilfillan, S.M.V., 2017. The influence of oxygen isotope exchange between CO2 and H2O in natural CO2-rich spring waters: Implications for geothermometry. Applied Geochemistry 84, 173–186. https://doi.org/10.1016/j.apgeochem.2017.06.012

Lara, L., Moreno, H.R., 2004. Geología del area Liquiñe - Neltume, regiones de La Araucanía y de Los Lagos, Escala 1:100.000. Santiago.

Lara, L.E., Cembrano, J., Lavenu, a., 2008. Quaternary Vertical Displacement along the Liquiñe-Ofqui Fault Zone: Differential Uplift and Coeval Volcanism in the Southern Andes? International Geology Review 50, 975–993. https://doi.org/10.2747/0020-6814.50.11.975

Melnick, D., Rosenau, M., Folguera, A., Echtler, H., 2006. Neogene tectonic evolution of the Neuquén Andes western flank (37–39°S). Special Paper 407: Evolution of an Andean Margin: A Tectonic and Magmatic View from the Andes to the Neuquén Basin (35°-39°S Lat). Geological Society of America, 73–95. https://doi.org/10.1130/2006.2407(04)

Moeck, C., Radny, D., Borer, P., Rothardt, J., Auckenthaler, A., Berg, M., Schirmer, M., 2016. Multicomponent statistical analysis to identify flow and transport processes in a highly-complex environment. Journal of Hydrology 542, 437–449. https://doi.org/10.1016/j.jhydrol.2016.09.023

Moya, C.E., Raiber, M., Taulis, M., Cox, M.E., 2015. Hydrochemical evolution and groundwater flow processes in the Galilee and Eromanga basins, Great Artesian Basin, Australia: A multivariate statistical approach. Science of The Total Environment 508, 411–426. https://doi.org/10.1016/J.SCITOTENV.2014.11.099

Munizaga, F., Herve, F., Drake, R., Pankhurst, R.J., Brook, M., Snelling, N., 1988. Geochronology of the Lake Region of south-central Chile (39°–42°S): Preliminary results. Journal of South American Earth Sciences 1, 309–316. https://doi.org/10.1016/0895-9811(88)90009-0

Negri, A., Daniele, L., Aravena, D., Muñoz, M., Delgado, A., Morata, D., 2018. Decoding fjord water contribution and geochemical processes in the Aysen thermal springs (Southern Patagonia, Chile). Journal of Geochemical Exploration 185, 1–13. https://doi.org/10.1016/J.GEXPLO.2017.10.026

Newell, D.L., Jessup, M.J., Cottle, J.M., Hilton, D.R., Sharp, Z.D., Fischer, T.P., 2008. Aqueous and isotope geochemistry of mineral springs along the southern margin of the Tibetan

plateau: Implications for fluid sources and regional degassing of CO_2. Geochemistry, Geophysics, Geosystems 9, n/a-n/a. https://doi.org/10.1029/2008GC002021

Patterson, J.W., Driesner, T., Matthai, S., Tomlinson, R., 2018. Heat and Fluid Transport Induced by Convective Fluid Circulation Within a Fracture or Fault. Journal of Geophysical Research: Solid Earth 123, 2658–2673. https://doi.org/10.1002/2017JB015363

Pérez-Flores, P., Cembrano, J., Sánchez-Alfaro, P., Veloso, E., Arancibia, G., Roquer, T., 2016. Tectonics, magmatism and paleo-fluid distribution in a strike-slip setting: Insights from the northern termination of the Liquiñe-Ofqui fault System, Chile. Tectonophysics 680, 192–210. https://doi.org/10.1016/j.tecto.2016.05.016

Reyes, A.G., Christenson, B.W., Faure, K., 2010. Sources of solutes and heat in low-enthalpy mineral waters and their relation to tectonic setting, New Zealand. Journal of Volcanology and Geothermal Research 192, 117–141. https://doi.org/10.1016/j.jvolgeores.2010.02.015

Roquer, T., Arancibia, G., Rowland, J., Iturrieta, P., Morata, D., Cembrano, J., 2017. Fault-controlled development of shallow hydrothermal systems: Structural and mineralogical insights from the Southern Andes. Geothermics 66, 156–173. https://doi.org/10.1016/j.geothermics.2016.12.003

Rosenau, M., Melnick, D., Echtler, H., 2006. Kinematic constraints on intra-arc shear and strain partitioning in the southern Andes between 38°S and 42°S latitude. Tectonics 25, n/a-n/a. https://doi.org/10.1029/2005TC001943

Roulleau, E., Tardani, D., Vlastelic, I., Vinet, N., Sanchez, J., Sano, Y., Takahata, N., 2018. Multi-element isotopic evolution of magmatic rocks from Caviahue-Copahue Volcanic Complex (Chile-Argentina): Involvement of mature slab recycled materials. Chemical Geology 476, 370–388. https://doi.org/10.1016/J.CHEMGEO.2017.11.035

Sánchez, P., Pérez-Flores, P., Arancibia, G., Cembrano, J., Reich, M., 2013. Crustal deformation effects on the chemical evolution of geothermal systems: the intra-arc Liquiñe–Ofqui fault system, Southern Andes. International Geology Review 55, 1384–1400. https://doi.org/10.1080/00206814.2013.775731

Taillefer, A., Guillou-Frottier, L., Soliva, R., Magri, F., Lopez, S., Courrioux, G., Millot, R., Ladouche, B., Le Goff, E., 2018. Topographic and Faults Control of Hydrothermal Circulation Along Dormant Faults in an Orogen. Geochemistry, Geophysics, Geosystems. https://doi.org/10.1029/2018GC007965

Taillefer, A., Soliva, R., Guillou-Frottier, L., Le Goff, E., Martin, G., Seranne, M., 2017. Fault-Related Controls on Upward Hydrothermal Flow: An Integrated Geological Study of the Têt Fault System, Eastern Pyrénées (France). Geofluids 2017, 1–19. https://doi.org/10.1155/2017/8190109

Tardani, D., Reich, M., Roulleau, E., Takahata, N., Sano, Y., Pérez-Flores, P., Sánchez-Alfaro, P., Cembrano, J., Arancibia, G., 2016. Exploring the structural controls on helium, nitrogen and carbon isotope signatures in hydrothermal fluids along an intra-arc fault system.

Geochimica et Cosmochimica Acta 184, 193–211. https://doi.org/10.1016/j.gca.2016.04.031

Townend, J., Sutherland, R., Toy, V.G., Doan, M.-L., Célérier, B., Massiot, C., Coussens, J., Jeppson, T., Janku-Capova, L., Remaud, L., Upton, P., Schmitt, D.R., Pezard, P., Williams, J., Allen, M.J., Baratin, L.-M., Barth, N., Becroft, L., Boese, C.M., Boulton, C., Broderick, N., Carpenter, B., Chamberlain, C.J., Cooper, A., Coutts, A., Cox, S.C., Craw, L., Eccles, J.D., Faulkner, D., Grieve, J., Grochowski, J., Gulley, A., Hartog, A., Henry, G., Howarth, J., Jacobs, K., Kato, N., Keys, S., Kirilova, M., Kometani, Y., Langridge, R., Lin, W., Little, T., Lukacs, A., Mallyon, D., Mariani, E., Mathewson, L., Melosh, B., Menzies, C., Moore, J., Morales, L., Mori, H., Niemeijer, A., Nishikawa, O., Nitsch, O., Paris, J., Prior, D.J., Sauer, K., Savage, M.K., Schleicher, A., Shigematsu, N., Taylor-Offord, S., Teagle, D., Tobin, H., Valdez, R., Weaver, K., Wiersberg, T., Zimmer, M., 2017. Petrophysical, Geochemical, and Hydrological Evidence for Extensive Fracture-Mediated Fluid and Heat Transport in the Alpine Fault's Hanging-Wall Damage Zone. Geochemistry, Geophysics, Geosystems 18, 4709–4732. https://doi.org/10.1002/2017GC007202

Vallejos, A., Díaz-Puga, M.A., Sola, F., Daniele, L., Pulido-Bosch, A., 2015. Using ion and isotope characterization to delimitate a hydrogeological macrosystem. Sierra de Gádor (SE, Spain). Journal of Geochemical Exploration 155, 14–25. https://doi.org/10.1016/j.gexplo.2015.03.006

Wrage, J., Tardani, D., Reich, M., Daniele, L., Arancibia, G., Cembrano, J., Sánchez-Alfaro, P., Morata, D., Pérez-Moreno, R., 2017. Geochemistry of thermal waters in the Southern Volcanic Zone, Chile – Implications for structural controls on geothermal fluid composition. Chemical Geology 466, 545–561. https://doi.org/10.1016/J.CHEMGEO.2017.07.004